JOURNAL OF APPLIED CRYSTALLOGRAPHY

ISSN 1600-5767

Received 29 December 2020
Accepted 11 April 2021

Edited by D. I. Svergun, European Molecular Biology Laboratory, Hamburg, Germany

Keywords: wavelength-resolved neutron transmission; Bragg edge; crystallographic texture; material properties.

A novel method to obtain integral parameters of the orientation distribution function of textured polycrystals from wavelength-resolved neutron transmission spectra

Miguel Angel Vicente Alvarez,[a,b]* Victor Laliena,[c] Florencia Malamud,[a,b] Javier Campo[c] and Javier Santisteban[b]

[a]Departamento de Física de Neutrones, Comisión Nacional de Energía Atómica CNEA/CONICET, 9500 Bustillo, SC de Bariloche, Rio Negro, 8400, Argentina, [b]Laboratorio Argentino de Haces de Neutrones, Comisión Nacional de Energía Atómica CNEA/CONICET, 9500 Bustillo, SC de Bariloche, Rio Negro, 8400, Argentina, and [c]Instituto de Nanociencia y Materiales de Aragón and Departamento de Física de la Materia Condensada, Facultad de Ciencias, CSIC – Universidad de Zaragoza, Calle de Pedro Cerbuna 12, Zaragoza, 50009, Spain. *Correspondence e-mail: m.a.vicente@cab.cnea.gov.ar

A novel method to estimate integral parameters of the orientation distribution function (ODF) in textured polycrystals from the wavelength-resolved neutron transmission is presented. It is based on the expression of the total coherent elastic cross section as a function of the Fourier coefficients of the ODF. This method is broken down in detail for obtaining Kearns factors in hexagonal crystals, and other material properties that depend on the average of second- and fourth-rank tensors. The robustness of the method against three situations was analyzed: effects of sample misalignment, of cutoff value l_{max} of the series expansion and of experimental standard deviation. While sample misalignment is shown not to be critical for the determination of Kearns factors and second-order-rank properties, it can be critical for fourth-rank and higher-order tensor properties. The effect of the cutoff value on the method robustness is correlated to the standard deviation of the experimental data. In order to achieve a good estimation of the Fourier coefficients, it is recommended that the experimental standard deviation be around 3–5% of the total scattering cross section of the material for the method to be stable. The method was applied for the determination of Kearns factors from transmission measurements performed at the instrument ENGIN-X (ISIS) on a Zr–2.5 Nb pressure tube along two sample directions and was shown to be able to estimate Kearns factors with an error below 5%.

1. Introduction

The use of neutron transmission at pulsed neutron sources as a tool for materials characterization has shown recent advances that profit from the energy resolution provided by the time-of flight technique. This was accompanied with the development of a sound theoretical background (Santisteban *et al.*, 2001) and software (Vogel, 2000; Sato *et al.*, 2011). The development of novel detectors combining high spatial and time-of-flight resolution has opened the possibility of novel analytical applications in neutron imaging to different areas of materials science (Woracek *et al.*, 2018). A few examples assessed the possibility of performing 3D imaging (tomography) of phase volumes (Woracek *et al.*, 2014) or strain (Wensrich *et al.*, 2016) by analyzing the energy dependence of transmission images. Wavelength-resolved imaging techniques have also been applied to steady-state reactors, with the use of a system of

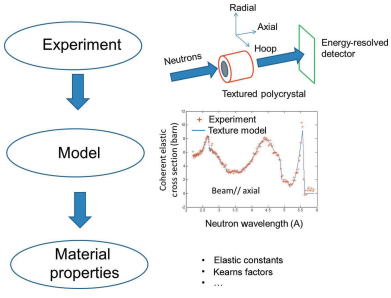

choppers (Strobl *et al.*, 2011) or double-crystal monochromators (Treimer *et al.*, 2006). The energy resolution of the instruments currently implemented at reactors (∼3% wavelength resolution) is still an order of magnitude worse than that found in pulsed sources (0.4% wavelength resolution).

Energy-resolved neutron tomography has been successfully applied for the case of crystalline-phase-fraction determination (Carminati *et al.*, 2020). However, obtaining spatial information for strain, particle size and orientation from neutron tomography is a more complex task. For strain and texture analysis, the application of traditional reconstruction methods fails because of the directional nature of these parameters, resulting in a voxel within the sample having a cross section that varies with viewing direction. In the traditional reconstruction methods, an isotropic total cross section is assumed, and hence it remains constant for all orientations of the object explored by the neutron. It is clear that a better understanding of the transmission models is necessary to improve tomographic reconstruction capabilities.

The effect of texture on neutron total cross section comes through the coherent elastic term. In the case of polycrystalline materials with small grain size (typically <5 µm) the kinematic approximation of diffraction is good, and closed expressions of the coherent elastic contribution in terms of texture can be obtained (Santisteban, Edwards & Stelmukh, 2006). In that pioneering paper it is shown that the previous expression obtained by Fermi for powder samples (Fermi *et al.*, 1947) can be extended to textured materials by the inclusion of a multiplicative factor for each Bragg edge. This factor accounts for the difference of volume fraction under diffraction in the case of a textured material compared with a powder, which is evaluated as a line integral along the pole figure of each Bragg edge. This expression was **found to be in good agreement** with experimental measurements performed on materials with quite different crystal structure and crystallographic texture (Santisteban, Edwards & Stelmukh, 2006; Malamud *et al.*, 2014). In a recent paper, a compact expression for the coherent elastic cross section was derived for textured polycrystals (Laliena *et al.*, 2020) This expression was deduced by analytical integration of the expression proposed by Santisteban, Edwards & Stelmukh (2006) for the Fourier expansion of the orientation distribution function (ODF), and is shown to be more efficient from a computational point of view, with a drastic reduction in computing time. The coherent elastic cross section term is then reduced to a summation of functions weighted by the Fourier coefficients of the ODF. In principle, this formulation opens new possibilities to incorporate texture into current tomographic reconstruction methods.

Although it is clear that the neutron transmission in textured materials can be computed with good accuracy once the ODF is known, up to now the inverse problem, *i.e.* obtaining the texture of the material from transmission experiments, has not been solved. The first attempts involved the inclusion of correction factors, like the March–Dollase formulation, in Rietveld refinement analysis of transmission data (Vogel, 2000; Sato *et al.*, 2011). These factors, however, are only a measure of the degree of departure of the experimental data from what is expected to occur with a powder sample, like an anisotropy factor. A more sophisticated approach involves using the height of the Bragg edge as a measure of the fraction of crystals with their plane normal parallel to the beam direction (Malamud, 2016). This method, though, does not take account of the complex dependence of the transmission data just after the Bragg edge, which depends on the actual texture of the material. The aim of this work is to explore the real capabilities of obtaining general texture parameters from transmission data, by proposing a method based on the evaluation of the total coherent elastic cross section in terms of the Fourier coefficients of the ODF. This work is organized as follows: In the next section we explain how the coherent elastic cross section is obtained from transmission experiments; then the inversion method is presented, from which it follows that in order to fully determine the ODF from transmission experiments a very large number of incidence directions must be analyzed simultaneously, as occurs in diffraction experiments. However, it will be shown that, when the focus is on obtaining integral parameters of the ODF (from which physical properties of the material can be deduced), it is sufficient to measure the transmission along a very reduced number of directions. This is the case of Kearns factors in hexagonal crystals or physical properties that depend on the average of second- and fourth-rank tensors, like electrical conductivity or elastic stiffness. For these cases, measurement of neutron transmission along a reduced number of incidence directions can still provide good estimations of integral or second-rank tensor properties. In Section 4 the robustness of the method is explored for the cases of sample misalignment, the cutoff value of the series expansion and the experimental standard deviation. Finally, in Section 5 the method is applied to obtain Kearns factors for the three principal directions of a tube made of a Zr alloy, from neutron transmission measurements performed at the instrument ENGIN-X along two different directions.

2. From neutron transmission experiment to total elastic coherent cross section

Experimentally, the determination of the transmitted energy-resolved neutron spectrum consists of measuring the spectroscopic transmission of the specimen, $T(\lambda)$, by comparing the signal recorded by a detector when the sample is in the beam, $i(\lambda)$, with the signal recorded for the direct neutron beam, $i_0(\lambda)$:

$$T(\lambda, \boldsymbol{\tau}) = i(\lambda, \boldsymbol{\tau})/i_0(\lambda), \tag{1}$$

where $\boldsymbol{\tau}$ indicates the direction of the transmitted neutron beam in the coordinate system of the sample. Within the kinematical theory of diffraction for polycrystalline materials, this transmission is directly related to the microscopic total cross section $\sigma_{\rm tot}(\lambda, \boldsymbol{\tau})$ of a unit cell of the material by

$$T(\lambda, \boldsymbol{\tau}) = \exp\left[-Nb\sigma_{\rm tot}(\lambda, \boldsymbol{\tau})\right], \tag{2}$$

where b is the thickness of the specimen along the neutron beam direction and N is the number of unit cells per unit volume. The total cross section includes all processes that remove neutrons from the incident beam, *i.e.* Bragg reflection, diffuse scattering and absorption. For the thermal/cold range the absorption contribution $\sigma_A(\lambda)$ is given by

$$\sigma_A(\lambda) = \sigma_{abs}(\lambda/\lambda_0) \tag{3}$$

with σ_{abs} the microscopic absorption cross section of the atom at the wavelength λ_0 (typically λ_0 = 1.8 Å). The diffuse scattering contribution $\sigma_s(\lambda)$ includes a combination of incoherent scattering processes and inelastic scattering and, like $\sigma_A(\lambda)$, is largely independent of the incident beam direction and has a smooth dependence on neutron wavelength. Theoretical expressions to calculate this contribution have been given by Granada (1984) and can be found in the appendix of the article by Malamud & Santisteban (2016).

Finally, the experimental total cross section component due to Bragg reflection $[\sigma_{el,coh}(\lambda, \boldsymbol{\tau})]$ along a specific specimen direction $\boldsymbol{\tau}$ can be empirically extracted from the measured $T(\lambda, \boldsymbol{\tau})$ simply by

$$\sigma_{el,coh}(\lambda, \boldsymbol{\tau}) = -\frac{1}{Nb}\ln[\,T(\lambda, \boldsymbol{\tau})] - \sigma_s(\lambda) - \sigma_A(\lambda). \tag{4}$$

3. Inversion method

The method for obtaining texture parameters from imaging experiments is based on an expression derived for the total neutron elastic coherent cross section in terms of the Fourier coefficients of the ODF. This expression was obtained after analytical integration of the differential coherent elastic cross section (Laliena *et al.*, 2020). For clarity, some basic formulae from this paper are here recalled.

The ODF, $f(g)$, can be expanded in a Fourier series as

$$f(g) = \sum_{l=0}^{\infty}\sum_{m=-l}^{l}\sum_{n=-l}^{l} C_l^{m,n} D_l^{m,n}(g), \tag{5}$$

where $D_l^{m,n}(g)$ are the Wigner D matrices [see Appendix A of Laliena *et al.* (2020)]. Orientation $g = (\alpha, \beta, \gamma)$ is defined by the following sequence of rotations in Euler space: $g_{\hat{\mathbf{z}}}(\alpha) g_{\hat{\mathbf{y}}}(\beta) g_{\hat{\mathbf{z}}}(\gamma)$, where $g_{\hat{\mathbf{n}}}(\psi)$ denotes rotation of an angle ψ around the $\hat{\mathbf{n}}$ direction. With this convention, the Fourier coefficients are calculated as

$$C_l^{m,n} = (2l+1)\int_{SO(3)} D_l^{m,n}(g)^* f(g)\,\mathrm{d}g \tag{6}$$

with $\mathrm{d}g = \sin\beta\,\mathrm{d}\alpha\,\mathrm{d}\beta\,\mathrm{d}\gamma$. The superscript * stands for the complex conjugate and the integration is performed over the whole Euler space. The Wigner matrices are given by

$$D_l^{m,n}(\alpha, \beta, \gamma) = \exp(-im\alpha)\, d_l^{mn}(\cos\beta)\exp(in\gamma). \tag{7}$$

With this definition of the Fourier coefficients and the property of Wigner matrices $D_l^{m,n} = D_l^{-m,-n*}$, reality of f implies $C_l^{m,n} = C_l^{-m,-n*}$. Then, the following expression for the total elastic coherent cross section of a single-phase textured material is obtained:

$$\sigma_{el,coh}(\lambda, \boldsymbol{\tau}) = \frac{N(2\pi)^3}{k^3}\sum_{\mathbf{G}}\frac{k}{2G}\left|F_{\mathbf{G}}\right|^2\Theta\left(1-\frac{G}{2k}\right) \times \sum_{l=0}^{\infty}\frac{4\pi}{2l+1}P_l\left(\frac{G}{2k}\right)\sum_{m=-l}^{l}\sum_{n=-l}^{l} C_l^{m,n}\, Y_l^n(\hat{\boldsymbol{G}})\, Y_l^m(\boldsymbol{\tau})^*, \tag{8}$$

where $k = 2\pi/\lambda$, $\mathbf{G}$ is **the reciprocal lattice vector** with modulus G, $|F_{\mathbf{G}}|^2$ is the square of the structure factor for the vector $\mathbf{G}$, $\Theta(x)$ is the Heaviside function, $P_l(x)$ is the Legendre polynomial of order l and Y_l^n are spherical harmonics.

Equation (8) can be written in the following form:

$$\sigma_{el,coh}(\lambda, \boldsymbol{\tau}) = \bar{\boldsymbol{B}}\,\bar{\boldsymbol{A}} = \sum_{l=0}^{\infty}\sum_{n=-1}^{l} B_{ln}\, A_{ln}, \tag{9a}$$

where

$$B_{ln}(\lambda) = \frac{2N(2\pi)^4}{v_0 k^3}\sum_{\mathbf{G}}\frac{k}{2G}\left|F_{\mathbf{G}}\right|^2\Theta\left(1-\frac{G}{2k}\right) \times \frac{1}{2l+1}P_l\left(\frac{G}{2k}\right)Y_l^n(\hat{\mathbf{G}}), \tag{9b}$$

$$A_{ln}(\boldsymbol{\tau}) = \sum_{m=-l}^{l} C_l^{m,n}\, Y_l^m(\boldsymbol{\tau})^*. \tag{9c}$$

In the case of a real experiment with a fixed incident beam direction $\boldsymbol{\tau}$, the transmission spectrum is measured along a wavelength range $[\lambda_{min}, \lambda_{max}]$ with a certain binning step. As functions B_{ln} only depend on λ, they can be evaluated for the same values of λ for which experimental data are available. In this context, equation (9*a*) can then be interpreted as the expansion of $\sigma_{el,coh}$ as a linear combination of vectors B_{ln} with A_{ln} the vector coefficients, these coefficients being dependent on the direction of the incident beam ($\boldsymbol{\tau}$).

Vectors B_{ln} depend on neutron wavelength and crystal structure through the structure factor and the summation over the reciprocal space vectors $\mathbf{G}$. Vectors B_{ln} are real since the summation in equation (9*b*) includes terms with $\mathbf{G}$ and $-\mathbf{G}$. Crystal symmetry operations must maintain this term unaltered; then B_{ln} vanishes for some values of (l, n). For example, in the case of a hexagonal crystal, the sixfold symmetry imposes that n must be a multiple of 6; the reflection operators requires that l must be odd, so the first nonzero vectors are B_{00}, B_{20} and B_{40}. For l = 6, three vectors are nonzero: B_{6-6}, B_{60} and B_{66}. Note that the relation $B_{ln} = B_{l-n}$ holds for all l and n, reducing considerably the number of linearly independent vectors B_{ln}. Fig. 1 shows the first non-vanishing B vectors for the α-Zr hexagonal phase as a function of neutron wavelength λ. The B_{00} curve was divided by 10 to make it comparable to the other curves, and it is proportional to the cross section expected for a random powder sample. All of these curves are piecewise continuous functions that vanish for $\lambda > 2d_{10\bar{1}0}$, which corresponds to the Bragg edge with the highest d spacing. The discontinuity points appear for $\lambda = 2d_{hkl}$, with d_{hkl} the spacing of the crystal planes under diffraction.

On the other hand, coefficients A_{ln} depend on the impinging direction $\boldsymbol{\tau}$ and on the crystallographic texture of the sample, through the ODF Fourier coefficients $C_l^{m,n}$. From equation (9*c*) and the property of the Fourier coefficients $C_l^{m,n} = C_l^{-m,-n*}$ it is straightforward to show that $A_{ln}^* = A_{l-n}$. This relation together with the fact that $B_{ln} = B_{l-n}$ guarantees the reality of $\sigma_{\rm el,coh}$. Note that A_{ln} are a combination of Fourier coefficients of order l. This is particularly important for material properties that only depend on the value of the Fourier coefficients of a given l order. This is the case for integral parameters of the ODF, like Kearns factors in hexagonal crystals (only depend on coefficients of order 2), or averaged elastic constants of a textured material (only depend on coefficients of order 4). In those cases, a good estimation of the material properties would be obtained from a limited number of A_{ln}, as will be shown next.

The idea behind the inversion method is to find the best approximation of coefficients A_{ln} by linear inversion of equation (9*a*). To do this, it is necessary to rearrange the summation in equation (9*a*), eliminating all the null and redundant terms. This is equivalent to finding a set of vectors B_{ln} that are linearly independent. With this in mind, we define an order index $\gamma = (l, n)$ that includes only those (l, n) values for which $B_{ln} \neq 0$ and $n \geq 0$. Defining $B_\gamma = B_{ln}$ for $n = 0$ and $B_\gamma = 2B_{ln}$ for $n \geq 0$, equation (9*a*) reduces to

$$\sigma_{\rm el,coh}(\lambda, \boldsymbol{\tau}) = \sum_\gamma B_\gamma A_\gamma, \tag{10}$$

where the summation is over γ and A_γ is the real part of A_{ln}. The factor 2 in the definition of B_γ is necessary to account for the contribution to equation (10) of the terms in equation (9*a*) with $n < 0$. Note that by transforming equations (9*a*)–(10) all terms associated with the imaginary part of A_{ln} disappear. Therefore, equation (9*c*) can be rewritten as

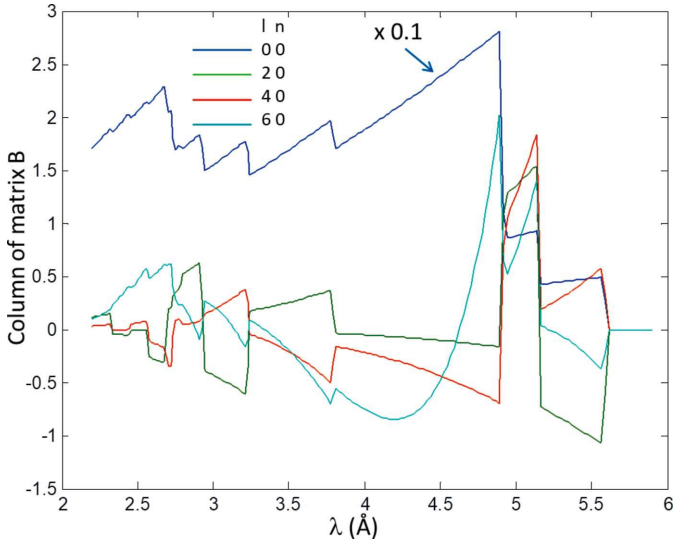

Figure 1
First vectors B_{ln}. The curve for $l = n = 0$ is proportional to the cross section expected for a random powder sample and it was divided by 10 to make it comparable to the other functions.

$$A_\gamma(\lambda, \boldsymbol{\tau}) = {\rm Re}\left[\sum_{m=-l}^{l} C_l^{m,n}\, Y_l^m(\boldsymbol{\tau})^*\right], \tag{11}$$

where Re(x) stands for the real part of x.

Defining the internal product as $\langle v, w\rangle = \int_{\lambda_{\rm min}}^{\lambda_{\rm max}} v(x)^* w(x)\,{\rm d}x$, we seek the minimization of the norm of the difference between $\sigma_{\rm el,coh}$ and a linear combination of vectors B_γ, $\min(\sigma_{\rm el,coh} - \sum_{\gamma=0}^{\gamma_{\rm max}} A_\gamma B_\gamma)$, with $\gamma_{\rm max}$ a cutoff value. For simplicity, this cutoff is chosen so as to include all the terms with $l \leq l_{\rm max}$. This minimization problem is straightforwardly solved by means of algebraic operations, leading to the following optimum solution for the coefficients:

$$\begin{pmatrix} A_1^{\rm opt} \\ \vdots \\ A_{\gamma_{\rm max}}^{\rm opt} \end{pmatrix} = \begin{pmatrix} \langle B_1, B_1\rangle & \dots & \langle B_1, B_{\gamma_{\rm max}}\rangle \\ \vdots & \vdots & \vdots \\ \langle B_{\gamma_{\rm max}}, B_1\rangle & \dots & \langle B_{\gamma_{\rm max}}, B_{\gamma_{\rm max}}\rangle \end{pmatrix}^{-1} \times \begin{pmatrix} \langle B_1, \sigma_{\rm el,coh}\rangle \\ \vdots \\ \langle B_{\gamma_{\rm max}}, \sigma_{\rm el,coh}\rangle \end{pmatrix}. \tag{12}$$

Linear independence of the B_γ vectors guarantees the existence of the inverse matrix in equation (12). The quality of fitting of $\sigma_{\rm el,coh}(\lambda, \boldsymbol{\tau})$ by the method will improve as the order $\gamma_{\rm max}$ (or $l_{\rm max}$) is increased. Coefficients $A_\gamma^{\rm opt}(\tau)$ **[should τ be bold throughout?]** obtained from equation (12) are dependent on τ since they are the solution of the problem for $\sigma_{\rm el,coh}$ measured along that direction. These coefficients are the key point of the inversion method since they are the fitting values of the experimental data and thus it is essential to determine their values with the highest accuracy. As coefficients $A_\gamma^{\rm opt}(\tau)$ are a linear combination of the Fourier coefficients of the ODF of the same l, to extract the values of $C_l^{m,n}$, it is necessary to invert equation (11). This can be done only if coefficients $A_\gamma^{\rm opt}(\tau)$ are available not for a single $\boldsymbol{\tau}$ but for a set of different beam directions. For each incident direction $\boldsymbol{\tau}$, equation (12) can be applied as an independent problem. If the procedure is repeated for beam directions $\boldsymbol{\tau}_1 \dots \boldsymbol{\tau}_i$, a set of optimum values $[A_\gamma^{\rm opt}(\tau_1) \dots . A_\gamma^{\rm opt}(\tau_i)]$ can be obtained and then be used as input to deduce the Fourier coefficients $C_l^{m,n}$ by inversion of equation (11). Clearly, if the intention is to obtain the values of coefficients $C_l^{m,n}$, inversion of equation (11) requires at least the same number of measurement directions as the number of non-vanishing Fourier coefficients of order l (both real and imaginary parts). This number increases drastically with l, implying that to have a good description of the ODF ($l \simeq 15$) from transmission data a huge number of sample rotations are necessary, probably similar to the number needed to have a good coverage of the pole figures in diffraction experiments. On the other hand, as mentioned before, if the object of this method is to obtain integrated values of the ODF (represented by a combination of $C_l^{m,n}$ with $l < 5$), a reduced set of τ would be sufficient. In the next section we will discuss the cases of Kearns factors in hexagonal crystal structures, second-rank tensors and elastic constants.

3.1. Determination of integral parameters of the ODF

3.1.1. Kearns factors in hexagonal crystals. It is common practice to define integral values of the crystallographic texture to compare the effect on texture of different processing routes. In the case of hexagonal crystal structures, like α-Zr, Kearns factors are commonly used (Kearns, 2001). These factors serve to evaluate averaged material properties when these properties take different values when measured along the c axis of the hexagons and normal to this direction. Let us assume that the property of interest (for example thermal expansion) depends on the angle β formed by the c axis of the hexagons with a reference direction of the sample $\hat{\mathbf{i}}$ (rolling direction, normal direction *etc*.) as follows:

$$P_{\mathrm{Ref}} = P_{(0001)} \cos^2 \beta + P_{(0001)\perp} \sin^2 \beta, \tag{13}$$

where $P_{(0001)}$ and $P_{(0001)\perp}$ are the values of the property along the c axis and normal to it, respectively. It is straightforward to show that the average value of this property for the whole material considering texture is given by

$$\langle P_{\mathrm{Ref}} \rangle = \mathrm{KF}_i P_{(0001)} + (1 - \mathrm{KF}_i) P_{(0001)\perp}, \tag{14}$$

where KF_i are defined as the Kearns factor corresponding to sample direction $\hat{\mathbf{i}}$. These factors are calculated as

$$\mathrm{KF}_i = \int_0^{\pi/2} I^{0001}(\beta) \sin\beta \cos^2\beta \, \mathrm{d}\beta, \tag{15}$$

where I^{0001} is the integral of the normalized (0001) pole figure over the line forming an angle β with the $\hat{\mathbf{i}}$ direction. In this expression $I^{0001}(\beta)\sin\beta\,\mathrm{d}\beta$ represents the fraction of grains in the material with an angle β between their c axis and $\hat{\mathbf{i}}$ (Malamud *et al.*, 2018). In general, Kearns factors for the three principal directions of the sample are reported: axial ($\mathrm{KF_A}$), hoop ($\mathrm{KF_H}$) and radial ($\mathrm{KF_R}$) in the case of tubing, and normal (ND), transverse (TD) and rolling (RD) directions in the case of flat-rolled products. Note that by construction these three factors sum to 1. Equation (15) can also be written as an integral over the whole Euler space of the ODF:

$$\mathrm{KF}_i = \int_{\mathrm{SO(3)}} f(g g_i^{-1}) \cos^2 \beta_g \, \mathrm{d}g, \tag{16}$$

where g_i^{-1} is the rotation needed to align the $\hat{\mathbf{i}}$ direction with the $\hat{\mathbf{z}}$ direction of the sample and $g = (\alpha, \beta, \gamma)$. This integral can be easily done by Fourier expansion of f and $\cos^2\beta_g$ and application of orthogonality relations of the generalized spherical harmonics. As $\cos^2\beta_g$ is expanded as a combination of spherical harmonics of order 2, only Fourier coefficients of the ODF with $l = 2$ remain after integration. The following expressions are obtained for the three KFs:

$$\mathrm{KF_{RD}} = \tfrac{1}{3} + \tfrac{8}{60}\mathrm{Re}\left(C_2^{0,0}\right), \tag{17a}$$

$$\mathrm{KF_{HD}} = \tfrac{1}{3} + \tfrac{8}{60}\mathrm{Re}\left[-\tfrac{1}{2}C_2^{0,0} - \left(\tfrac{3}{2}\right)^{1/2} C_2^{2,0}\right], \tag{17b}$$

$$\mathrm{KF_{AD}} = \tfrac{1}{3} + \tfrac{8}{60}\mathrm{Re}\left[-\tfrac{1}{2}C_2^{0,0} + \left(\tfrac{3}{2}\right)^{1/2} C_2^{2,0}\right]. \tag{17c}$$

It is clear from equations (17) that the three KFs sum to 1, and that if the texture is isotropic $C_2^{0,0} = C_2^{2,0} = 0$ and then $\mathrm{KF_{RD}} = \mathrm{KF_{HD}} = \mathrm{KF_{AD}} = \frac{1}{3}$, as expected. In equations (17) the following convention for the sample directions and Euler rotation is used: AD – x axis, HD – y axis and RD – z axis.

Kearns factors depend on the real part of the $C_2^{0,0}$ and $C_2^{2,0}$ Fourier coefficients, which can be obtained by inversion of equation (11) from the optimum values A_γ^{opt} with $l = 2$. Owing to the crystal symmetry of hexagonal crystals, the only term with $l = 2$ different from zero is A_{20}^{opt}. This means that in order to infer both $\mathrm{Re}(C_2^{0,0})$ and $\mathrm{Re}(C_2^{2,0})$ a set of at least two measurement directions must be included in the optimization procedure. In principle, these two directions are arbitrary, yet for the particular case of beam directions along the axial ($\boldsymbol{\tau}$ = [1, 0, 0]) and hoop ($\boldsymbol{\tau}$ = [0, 1, 0]) directions of the tube, equation (11) reduces to

$$\begin{bmatrix} A_{20}^{\mathrm{opt}}(\mathrm{AD}) \\ A_{20}^{\mathrm{opt}}(\mathrm{HD}) \end{bmatrix} = \begin{pmatrix} 0.3863 & -0.3154 \\ -0.3863 & -0.3154 \end{pmatrix} \begin{bmatrix} 2\mathrm{Re}(C_2^{2,0}) \\ \mathrm{Re}(C_2^{0,0}) \end{bmatrix}. \tag{18}$$

To obtain this equation, summation over m was rearranged considering that $\mathrm{Re}(C_2^{2,0}) = \mathrm{Re}(C_2^{-2,0})$. $\mathrm{Re}(C_2^{2,0})$ and $\mathrm{Re}(C_2^{0,0})$ can be obtained by inverting equation (18) once the values of $A_{20}^{\mathrm{opt}}(\mathrm{AD})$ and $A_{20}^{\mathrm{opt}}(\mathrm{HD})$ are determined and then replaced in equations (17) to evaluate the Kearns factors. Relations similar to equation (18) can be derived if different beam directions are used.

3.1.2. Averaged values of second-rank tensors. A large number of physical properties can be described by second-rank tensors, *e.g.* thermal expansion, optical refractive index, and electrical and thermal conductivity. In the case of a textured polycrystal, the macroscopic value of these physical properties is generally evaluated by averaging the single-crystal property over the whole grain ensemble. In terms of the ODF, this means integrating over the whole Euler space the single-crystal tensorial properties corresponding to each grain, but written in the sample reference system and weighted by $f(g)$. In the case of second-rank tensors, transformation of the single-crystal tensor is done by the left product of the orientation matrix g and right product of the orientation matrix g^{-1}. Integration can be done analytically by Fourier expansion of $f(g)$, and only terms with $l = 2$ remain (Bunge, 1982). Equation 13.78 of Bunge's book shows that each component of the macroscopic average can be written as a linear combination of Fourier coefficients with $l = 2$.

To obtain coefficients $C_2^{m,n}$ we proceed in a similar way as in the case of Kearns factors. Considering that for hexagonal and cubic crystals there are a total of five independent unknowns (including the real and imaginary parts of $C_2^{2,0}$ and $C_2^{1,0}$ and the real part of $C_2^{0,0}$) and that for each beam direction only A_{20} is accessible, to invert equation (11) a minimum of five non-equivalent measurement directions are needed. Taking the set of beam directions [1, 0, 0]; [0, 1, 0]; [0, 1, 1]; [1, 1, 0]; and [1, 0, 1], the following inversion matrix for the $C_2^{m,0}$ coefficients is obtained:

$$\begin{pmatrix} C_2^{2,0} \\ C_2^{1,0} \\ C_2^{0,0} \end{pmatrix} = \begin{pmatrix} 0.6472 + 0.6472i & -0.6472 + 0.6472i & 0 & -1.2944i & 0 \\ -0.6472i & 0.6472 & -1.2944i & 0 & 1.2944 \\ -1.5853 & -1.5853 & 0 & 0 & 0 \end{pmatrix} \times \begin{bmatrix} A_{20}^{\rm opt}(\tau_1) \\ A_{20}^{\rm opt}(\tau_2) \\ A_{20}^{\rm opt}(\tau_3) \\ A_{20}^{\rm opt}(\tau_4) \\ A_{20}^{\rm opt}(\tau_5) \end{bmatrix}. \quad (19)$$

The vector on the right of equation (19) is built from the experimental optimum values of $A_{20}^{\rm opt}$ obtained after fitting of the total cross section along the five directions $\boldsymbol{\tau}_1$–$\boldsymbol{\tau}_5$ mentioned above.

3.1.3. Averaged values of forth-rank tensors. The case of forth-rank tensors, like elastic stiffness or compliance, is similar to that discussed above when dealing with second-rank tensors. In this case, the average value of the crystal tensor over the Euler space is reduced to the contribution of the Fourier coefficients with $l = 4$. Therefore, for hexagonal crystals, a total of nine independent unknowns need to be determined (real and imaginary parts of $C_4^{4,0}$, $C_4^{3,0}$, $C_4^{2,0}$ and $C_4^{1,0}$ and the real part of $C_4^{0,0}$). As in the case of $l = 2$, the only coefficient A_4^n different from zero is A_4^0. So, in order to apply the inversion method, measurements along at least nine different incident directions must be made and a matrix system similar to that of equation (19) can be constructed. A proposal for such directions is [1, 0, 0]; [0, 1, 0]; [0, 1, 1]; [1, 1, 0]; [1, 0, 1]; [2, 1, 0]; [1, 2, 0]; [2, 0, 1]; and [0, 1, 2]. Note that during fitting of the experimental cross section not only optimum values of A_4^0 are obtained but also those of A_2^0. This means that, in the case of these nine different measurement directions, Fourier coefficients with both $l = 4$ and $l = 2$ can be inferred. In the case of $l = 2$, matrix system (19) can no longer be applied; however this can be solved by applying a least-squares minimization procedure.

4. Analysis on the robustness of the method

To check the applicability of the method, we have simulated ideal experiments, using equation (8) to evaluate the elastic coherent cross section from a known ODF. Then, this cross section was used as input to the inversion model. The case of a Zr–2.5 Nb pressure tube (hexagonal crystal phase, α-Zr) was chosen to generate the cross section.

The texture of this material was measured by neutron and synchrotron X-ray diffraction (Malamud *et al.*, 2018) and is shown in Fig. 2(*a*). The three principal directions of the tube are indicated in the pole figures: the center corresponds to the radial direction, the east to the hoop direction and the north to the axial direction. This texture is characterized by a $\langle 11\bar{2}0\rangle$ // AD fiber. This means that the $(10\bar{1}0)$ poles are aligned to the axial direction while the *c* axis of the hexagons is lying along the hoop–radial line. The intensity distribution along this fiber is not uniform, with a sharp maximum for the *c* axis along the hoop direction and a fast decrease of intensity for orientations rotated more than 20° apart. Fig. 2(*b*) shows how the modulus of the Fourier coefficients decreases with the harmonic order *l*. These coefficients were calculated using *MTEX* (Hielscher & Schaeben, 2008), a free texture toolbox in MATLAB language. As this texture is sharp, coefficients up to $l \simeq 20$ have a significant contribution to the series expansion of $f(g)$.

Fig. 3 shows the total coherent elastic cross section for three different beam directions. The lines in blue were calculated using the integral form of Santisteban, Edwards & Stelmukh (2006), while the red crosses are the result of equation (8) with $l_{\rm max} = 40$. The positions of the Bragg edges are also indicated in the figure. The marked change of $\sigma_{\rm el,coh}$ with the neutron

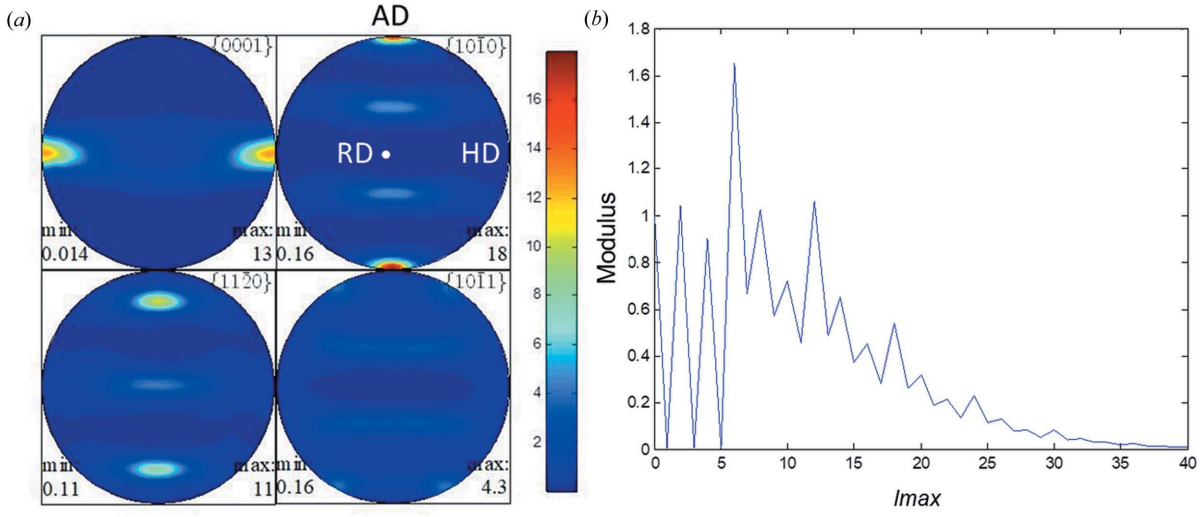

Figure 2
(*a*) Pole figures of a Zr–2.5 Nb pressure tube and (*b*) modulus of Fourier coefficients of the ODF as a function of the harmonic order $l_{\rm max}$.

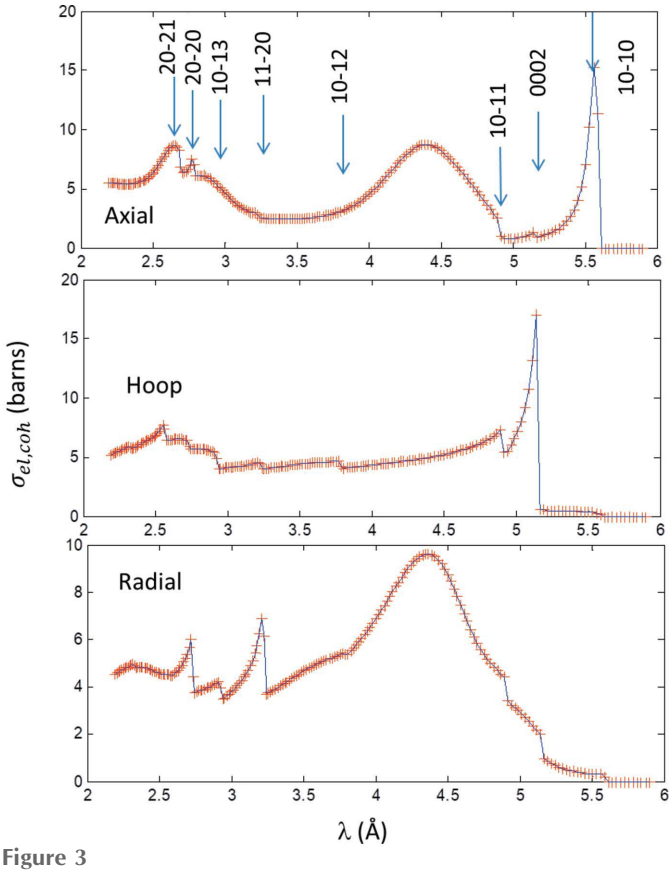

Figure 3
Comparison between the total elastic coherent cross section $\sigma_{el,coh}$ of the pressure tube along three different beam directions. The blue lines were calculated using the integral form of Santisteban, Edwards & Stelmukh (2006). The red crosses show the result of equation (8) using $l_{max} = 40$.

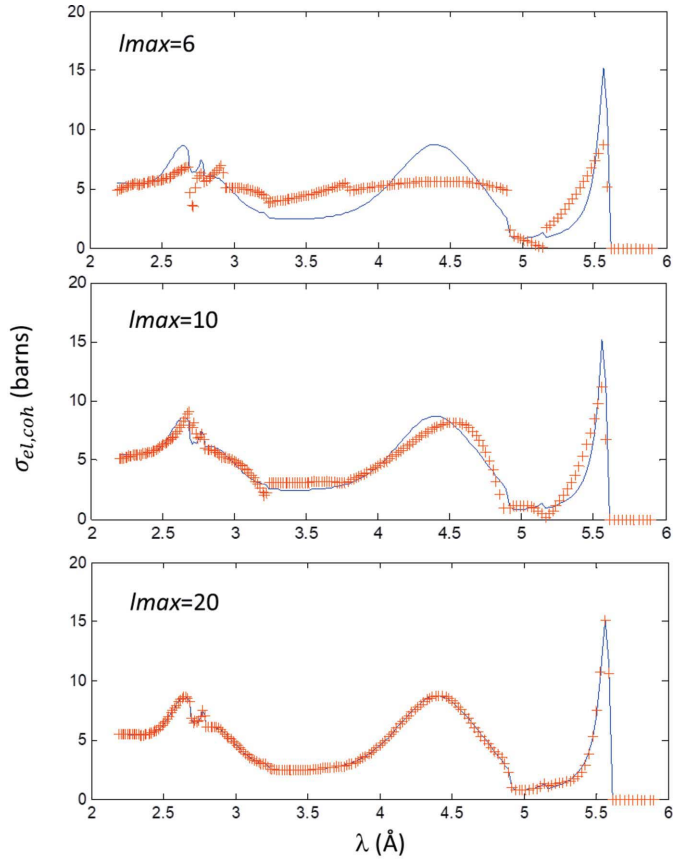

Figure 4
Comparison between input cross section (blue) and the cross section along the axial direction of the tube evaluated after applying the inversion method (red) for three different values of l_{max}.

beam direction is a consequence of the sharpness of the texture. The $(10\bar{1}0)$ Bragg edge is intense for the beam//axial direction, while it is almost negligible for the other two beam directions. This is because the height of each Bragg edge is proportional to the fraction of grains oriented with the corresponding plane normal parallel to the beam direction. The particular texture of this material shows a concentration of $(10\bar{1}0)$ poles along the axial direction and only a few poles oriented along the hoop or radial directions. Something similar occurs for the (0002) Bragg edge, where the most intense gap happens when the beam is along the hoop direction of the tube. For $\lambda > 5.5$ Å, $\sigma_{el,coh} = 0$, since diffraction is forbidden. For $\lambda < 2$ Å there is a superposition of contributions of Bragg edges and $\sigma_{el,coh}$ tends to a constant value.

The inversion method was used to obtain the optimum values A_γ^{opt} for l up to 6. Three different situations were analyzed: (1) effect of the cutoff l_{max}, (2) effect of sample misalignment and (3) effect of statistical uncertainties. In all cases the optimum values are compared with those obtained by direct evaluation of equation (11).

4.1. Effect of cutoff l_{max}

Considering that **the aim** of the inversion method is to determine the values of A_γ^{opt} for the lowest values of l, this raises the need to understand how these values depend on the cutoff value l_{max} used to invert equation (10). To analyze this point, we compare A_γ^{opt} for l up to 6 for different l_{max}. Figs. 4 and 5 show the results of the analysis for the case of a beam

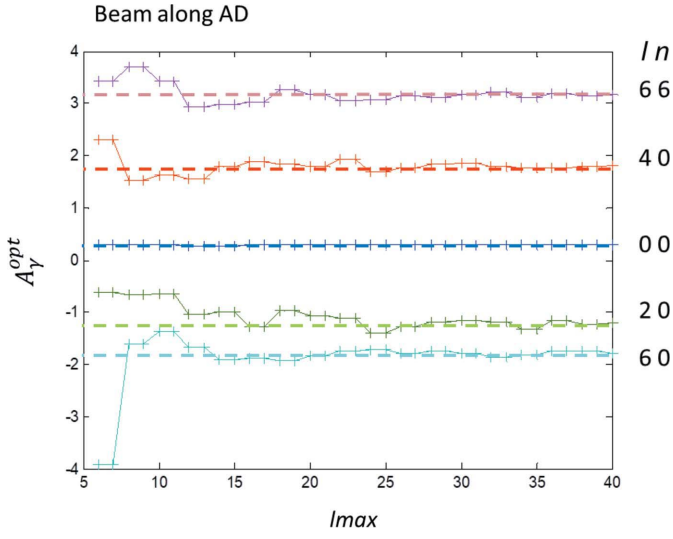

Figure 5
Evolution of the optimum values A_γ^{opt} with cutoff l_{max}. The dashed lines correspond to the values of A_γ for different l and n calculated from equation (11) using the Fourier coefficients of the ODF.

impinging along the axial direction of the tube. In Fig. 4 the elastic cross section used as input for the inversion model (in blue) is compared with the resulting cross section after inversion for three different l_{max} (crosses in red). In the case of $l_{max} = 6$ (five independent A_γs), the quality of fitting is poor. It improves considerably for $l_{max} = 10$ (nine independent A_γs), although some differences are still observed. For $l_{max} = 20$ (26 independent A_γs) the fitting is excellent. In Fig. 5 the evolution of the coefficients A_γ^{opt} is plotted as a function of l_{max}. The dashed lines correspond to the target values of A_γ, computed from equation (11) and using the Fourier coefficients of the ODF. For $l_{max} = 6$ the values of A_γ^{opt} differ from the target, for $l_{max} = 10$ the difference is reduced considerably and for $l_{max} > 15$ all A_γs are converged.

Clearly, the value of $l_{max} > 15$ at which convergence occurs must depend on the material texture. It is expected that this value must be higher for sharp textures than for soft textures.

4.2. Effect of sample misalignment

In the previous sections it was shown that for a fixed beam direction the inversion model has a good capacity to estimate the value of coefficients A_γ. In a real experiment, there are always uncertainties associated with sample positioning and alignment, principally due to effects of sample preparation and handling. Sample misalignment translates into uncertainties on the values of the different τs measured in the experiment, and thus on errors on the value of the matrix elements in equation (11). As this equation relates coefficients A_γ and coefficients $C_l^{m,n}$, uncertainties on τ produce errors on the determination of coefficients $C_l^{m,n}$, thus affecting the estimation of the material properties of interest. The idea of this section is to answer the following question: how precisely must a sample be aligned and rotated in order to obtain values of A_γ useful for material property estimation?

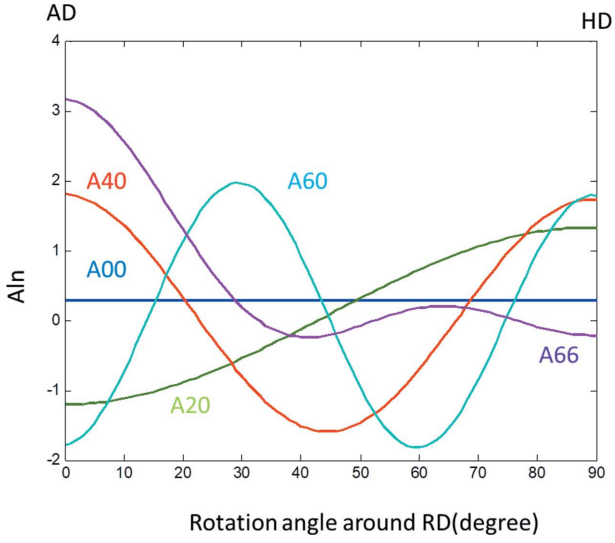

Figure 6
Variation of the first coefficients A_{ln} calculated from equation (11) for beam direction varying from AD to HD by rotation around the RD.

To carry out this study, we will focus on the variation of the first A_γ when the sample is rotated apart from a nominal direction, *i.e.* RD, AD and HD in a tube. As the inversion model proved to be able to estimate A_γ with high accuracy, we will work directly with the theoretical value of A_γ obtained from equation (11) for a known $C_l^{m,n}$.

In Fig. 6 we present the changes of A_γ (for $l \leq 6$) for a set of beam directions from the AD (rotation angle = 0) to the HD of the tube (rotation angle = 90°). These values were calculated from equation (11) with the $C_l^{m,n}$ of the pressure tube. Coefficient A_{00} is a constant, A_{20} varies smoothly from the AD to the HD, while higher-l coefficients change with the rotation angle in a more pronounced way. This is reasonable since, according to equation (11), coefficients of order l vary with the beam direction as a linear combination of Y_l^m functions. In particular, only a small variation of A_{20} occurs even for a beam direction 10° from the AD or HD direction of the tube This implies that in order to obtain physical quantities that depend on Fourier coefficients with $l = 2$ a rough sample alignment is enough; however, for properties associated with Fourier coefficients of order $l = 4$ or higher much care must be taken at the moment of sample positioning. Although these results were obtained for a particular imposed texture, that can be extrapolated to materials with other textures, since the major dependence with the rotation angle is through the Y_l^m functions. Obviously, the speed of change of parameters A_γ will be dependent on the sharpness of the texture. Soft textures will give rise to smooth changes while sharp textures will imply a more marked variation of the coefficients.

4.3. Effect of statistical uncertainties

Another aspect of great importance is the statistical uncertainty of the experimental data. To quantify its effect, we carry out the following exercise: we test the inversion model using as input to the model different cross sections that are generated as variants of an 'ideal' cross section by addition of a Gaussian random function. The 'ideal' cross section is the one presented in Fig. 4, obtained from equation (8) for the beam direction along the AD. The random function is used to simulate the experimental uncertainty typical of an experiment. The inversion method was then applied for these modified cross sections for different widths of the Gaussian function ($\Delta\sigma$). In all cases, the variation of the fitting coefficients A_γ^{opt} with the cutoff l_{max} used in the inversion model was studied. Note that the results presented in Fig. 4 can be seen as the case of zero Gaussian width.

Fig. 7 shows the results for three different widths $\Delta\sigma$: ±0.2, ±0.5 and ±1 barn (1 barn = 10^{-28} m^2). In terms of the coherent elastic cross section of Zr (6.44 barn), these three values represent relative uncertainties of the data of ±3, ±7.5 and ±15%, respectively. The results are presented as two graphs: at the top of each column the input cross section (red crosses) is compared with the cross section after fitting (blue curve) for $l_{max} = 40$; in the graphs at the bottom of each column the variation of the first A_γ^{opt} ($l \leq 6$) with the cutoff l_{max} is shown. In these plots a dashed lines is included to indicate

the target value (for $\Delta\sigma = 0$ as in Fig. 5). For low l_{max} the fit is not good. As l_{max} is increased, coefficients A_γ^{opt} tend to the target values. However, in contrast to what is observed in Fig. 5, even for the lowest values of $\Delta\sigma$ there is a limiting value of l_{max} above which all coefficients A_γ^{opt} different from A_{00} start to depart from the target value. Moreover, in the limiting case of $l_{max} \simeq 40$, the fitted coefficients A_γ^{opt} fall out of range. This behavior occurs because those terms in equation (10) with high l become increasingly important to adjust the oscillations introduced by the random function. The contribution of these high-l terms has to be compensated by the low-l terms to fit the experimental curve, which results in bias of A_γ^{opt} with low l. The analysis shows that there is a window of values of l_{max} for which the inversion method is reliable. For values of $l_{max} < 10$, fitting of the experimental data is poor and estimation of A_γ^{opt} is poor too; for values of l_{max} that are too high, the experimental statistical fluctuations impair a good estimation of A_γ^{opt}. Interestingly, the size of this window gets narrower as $\Delta\sigma$ increases. In the case of $\Delta\sigma = 0.2$ barn ($\pm 3\%$) the estimated A_γ^{opt} values remain close to the target value for $10 < l_{max} < 30$, while for $\Delta\sigma = 1$ barn ($\pm 15\%$) this window reduces to $14 < l_{max} < 20$ and the inversion method becomes unreliable.

This analysis shows the importance of the determination of the coherent elastic cross section with a low uncertainty. In this particular case, it is recommended that $\Delta\sigma$ is kept below 5% of the atomic coherent elastic cross section of the elements forming the material.

In a real experiment, the target value for coefficients A_γ is not available. Therefore, it is important to define a criterion to delimit the window of l_{max} for which the method is still reliable. One proposal is to plot the goodness of fit (calculated in this case as the sum of residuals per point) as a function of l_{max} and choose the value of l_{max} for which this value becomes similar to the experimental error $\Delta\sigma$. Note that the better the fitting the lower the value of the goodness of fit. On the other hand, $\Delta\sigma$ can be determined from the experimental values for short intervals where there is a smooth dependence of the coherent cross section on λ. This criterion is based on the fact that at the moment the goodness of fit becomes comparable to or smaller than the statistical error $\Delta\sigma$ the theoretical expression will be fitting the fluctuations produced by the experimental noise, thus impairing the convergence of coefficients A_γ^{opt}.

5. Application to a real experiment: determination of Kearns factors

The inversion method was applied to the case of a Zr–2.5 Nb pressure tube with the aim of obtaining Kearns factors from two independent neutron transmission measurements. The procedure consisted of the following steps: (1) derivation of the elastic coherent total cross section from the experimental transmission spectra, (2) application of the inversion method with increasing cutoff l_{max}, (3) evaluation of experimental noise ε and selection of the maximum value of l_{max} for which the results are reliable according to the criterion proposed in the previous section, (4) determination of parameters A_{20}, and (5) use of equations (11) and (12) to calculate the Kearns factors.

The neutron transmission measurements were performed on ENGIN-X at the ISIS Facility, UK (Santisteban, Daymond *et al.*, 2006), on a small specimen (10×20 mm along the axial and rolling directions, respectively) machined out of a Zr–2.5 Nb pressure tube. The texture of this tube is shown in Fig. 2. The measurements were obtained for two beam directions – along the hoop and the axial directions of the tube – using a

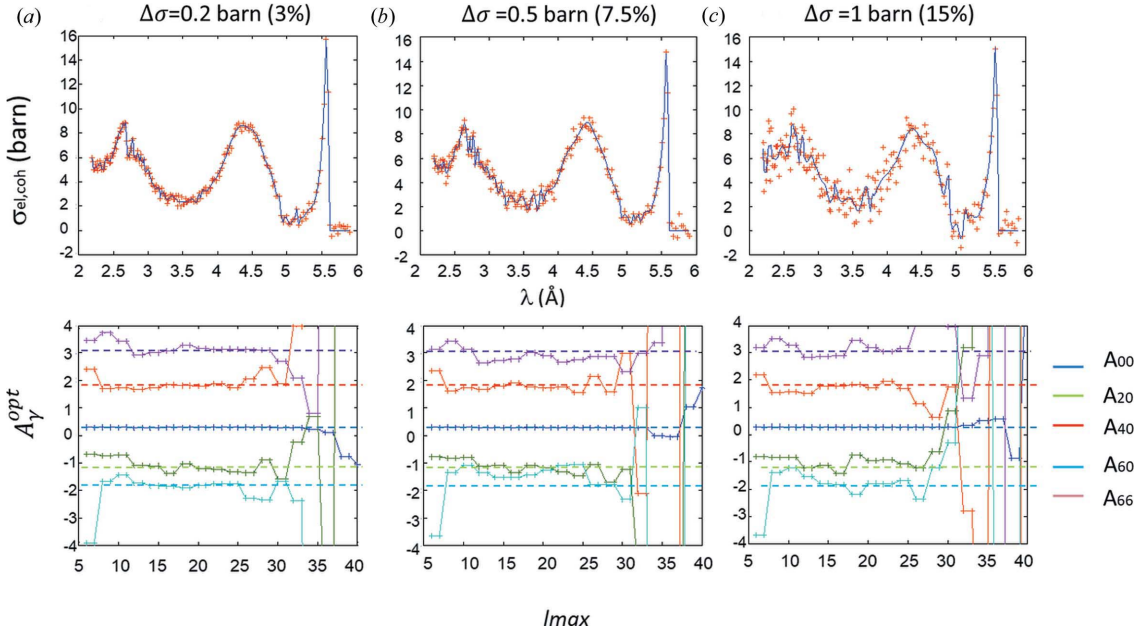

Figure 7
Effect of simulated experimental statistical uncertainty on the determination of the optimum A_γ^{opt} coefficients. Each column corresponds to the result for a different value of $\Delta\sigma$. At the top a comparison between the input curve (red crosses) and the result after fitting (blue curves) for $l_{max} = 40$ is presented. At the bottom the evolution of A_γ^{opt} with l_{max} is compared with the target values calculated from the ODF Fourier coefficients (dashed lines).

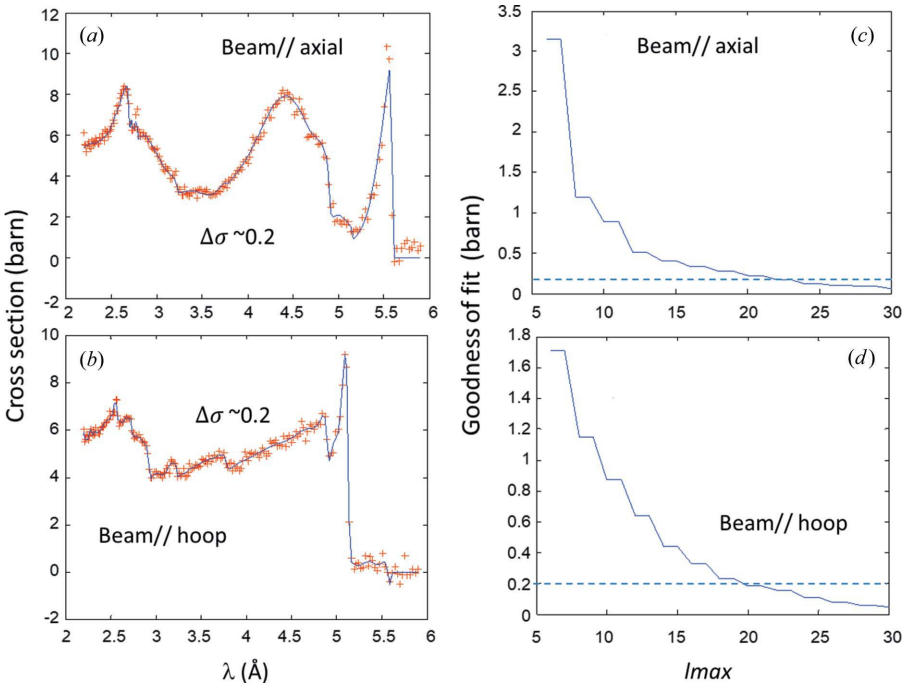

Figure 8
Fitting of the experimental points (red) after applying the inversion method for l_{max} = 20 (blue curves) for the beam (*a*) along the axial and (*b*) along the hoop direction. Evolution of the goodness of fit as a function of l_{max} for the beam (*c*) along the axial and (*d*) along the hoop direction of the tube. The dashed lines indicate the experimental standard deviation $\Delta\sigma$ for each case.

neutron beam area of 6 × 4 mm and an incident beam divergence optimized for texture measurement of ∼0.7 × 0.8° (horizontal × vertical). For each measurement the coherent total elastic cross section was derived using equation (4), after subtraction of the scattering and absorption contributions.

Figs. 8(*a*) and 8(*b*) show a comparison between the experimental elastic coherent cross section (in blue) and the calculated $\sigma_{el,coh}$ after applying the inversion method for a cutoff of l_{max} = 20 (in red) for the two measurement directions. The quality of the fit is excellent for both cases. The experimental noise $\Delta\sigma$ was estimated to be ±0.2 barns in both cases. In Figs. 8(*c*) and 8(*d*) the goodness of fit is plotted as a function of l_{max}. In these figures the horizontal dashed line shows the value of $\Delta\sigma$ = 0.2 barns. The goodness of fit decreases markedly as l_{max} increases and reaches a value of 0.2 barns for $l_{max} \simeq 23$ in the case of the beam along the axial direction and for $l_{max} \simeq 20$ for the beam along the hoop direction. In Fig. 9, the evolution of coefficients A_{00}, A_{20} and A_{40} with l_{max} is presented. The vertical dashed lines show the limiting value of l_{max} obtained from Figs. 8(*c*) and 8(*d*). For the beam along the axial direction [Fig. 9(*a*)] the evolution of coefficients A_{20} and A_{40} is smooth for values of l_{max} up to 23, and from there on this trend is broken and they start to increase markedly in size. Their behavior with l_{max} is similar to that shown in Fig. 7 when the effect of the experimental uncertainty was analyzed. Something similar occurs for the case of the beam along the hoop direction.

In order to estimate Kearns factors from these measurements, the experimental values of A_{20} were taken to be the average of the curves for l_{max} from 15 to 20 for the hoop direction and from 18 to 23 for the axial direction. With these values the real parts of the ODF C_2^{00} and C_2^{20} coefficients were obtained by inversion of equation (18) and then replaced in equations (17) to obtain the Kearns factors. Table 1 summarizes the results obtained after applying this method. The values calculated from the ODF are also included. A good agreement between the determined and the expected results is observed.

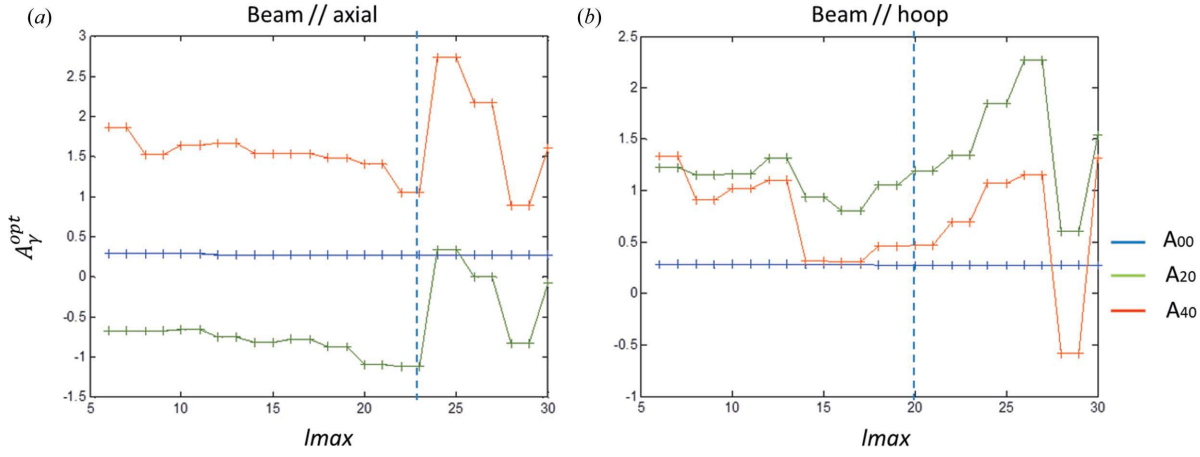

Figure 9
Evaluation of the optimum values A_γ^{opt} obtained from the experimental curves for different values of l_{max}. (*a*) Beam along the axial direction and (*b*) beam along the hoop direction. The vertical dashed lines indicate the value of l_{max} for which the goodness of fit is equal to the experimental standard deviation $\Delta\sigma$ determined from Figs. 8(*c*) and 8(*d*).

Table 1
Comparison between the Fourier coefficients of order $l = 2$ and Kearns factors obtained by the inversion method and from the ODF **[please check the number of decimal places of these values; the error should at least match the respective value, i.e. 1.1 ± 0.2 or 1.10 ± 0.15 intead of 1.1 ± 0.15]**.

	A_{20} axial	A_{20} hoop	$2\mathrm{Re}(C_2^{20})$	$\mathrm{Re}(C_2^{00})$	$\mathrm{KF_{Axial}}$	$\mathrm{KF_{Hoop}}$	$\mathrm{KF_{Radial}}$
Inversion method	-1.05 ± 0.1	1.1 ± 0.15	-2.78 ± 0.3	-0.1 ± 0.3	0.11 ± 0.02	0.57 ± 0.03	0.32 ± 0.04
ODF	−1.205	1.304	−3.2822	−0.1987	0.08	0.61	0.31

The Kearns factors derived from the experiment present a typical uncertainty of 0.03 and show values very close to those calculated from the ODF, especially considering that only two measurement directions were used for their determination.

6. Conclusions

A novel method to estimate integral parameters of the ODF of a polycrystalline material from energy-resolved neutron transmission measurements is presented. It is based on deriving an expression for the total coherent elastic cross section in terms of the Fourier coefficients describing the ODF. The procedure was specified to obtain the Kearns factors for hexagonal materials from only two transmission measurements. Expressions were presented to obtain also other material properties that depend on the average of second- and fourth-order tensors, which require measuring the transmission along a minimum of five and nine directions, respectively.

A generalization of the method can be applied to determine the complete ODF Fourier coefficients of any order l. However, the number of independent measurement directions must be increased as the order l becomes higher.

The robustness of the inversion method was explored by considering the effect of three parameters involved in the analysis on the resulting Fourier coefficients: the effect of sample misalignment, the choice of cutoff value $l_{\max}$ and the impact of the experimental uncertainty. While sample misalignment is not critical for the determination of Kearns factors and second-order-rank properties, it can be critical for fourth-rank and higher-order tensor properties. The choice of the cutoff value is directly linked to the standard deviation of the experimental data. In order to achieve a good estimation of the Fourier coefficients, it is recommended that the experimental standard deviation be around 3–5% of the total scattering cross section of the material. If this is not met, the method may become unstable.

The proposed method was tested through the determination of Kearns factors from time-of-flight neutron transmission spectra measured along the hoop and axial directions of a Zr–2.5 Nb pressure tube. The method proved to be capable of estimating Kearns factors with a typical uncertainty of 0.03.

Funding information

The following funding is acknowledged: Ministerio de Ciencia, Innovación y Universidades (Spain) (grant No. PGC-2018-099024-B-I00); Consejo Superior de Investigaciones Científicas (Spain) (grant No. I-COOP B20319); Aragon Regional Govenment (Spain) (grant No. E11_17R); Consejo Nacional de Investigaciones Científicas y Técnicas (CONICET), Argentina (grant No. PIP 11220150100487CO).

References

Bunge, H. J. (1982). *Texture Analysis in Materials Science: Mathematical Methods*. London: Butterworths.

Carminati, C., Strobl, M., Minniti, T., Boillat, P., Hovind, J., Morgano, M., Holm Rod, T., Polatidis, E., Valsecchi, J., Mannes, D., Kockelmann, W. & Kaestner, A. (2020). *J. Appl. Cryst.* **53**, 188–196.

Fermi, E., Sturm, W. J. & Sachs, R. G. (1947). *Phys. Rev.* **71**, 589–594.

Granada, J. R. (1984). *Z. Naturforsch.* **39**, 1160–1167.

Hielscher, R. & Schaeben, H. (2008). *J. Appl. Cryst.* **41**, 1024–1037.

Kearns, J. J. (2001). *J. Nucl. Mater.* **299**, 171–174.

Laliena, V., Vicente-Álvarez, M. Á. & Campo, J. (2020). *J. Appl. Cryst.* **53**, 512–529.

Malamud, F. (2016). PhD thesis, Instituto Balseiro, Bariloche, Argentina.

Malamud, F., Riffo, A. M., Alvarez, M. A. V., Vizcaino, P., Li, M. J., Liu, X., Vogel, S. C., Law, M., Sumin, V. V., Luzin, V., Vasin, R. N. & Santisteban, J. R. (2018). *J. Nucl. Mater.* **510**, 524–538.

Malamud, F. & Santisteban, J. R. (2016). *J. Appl. Cryst.* **49**, 348–365.

Malamud, F., Santisteban, J. R., Vicente Alvarez, M. A., Bolmaro, R., Kelleher, J., Kabra, S. & Kockelmann, W. (2014). *J. Appl. Cryst.* **47**, 1337–1354.

Santisteban, J. R., Daymond, M. R., James, J. A. & Edwards, L. (2006). *J. Appl. Cryst.* **39**, 812–825.

Santisteban, J. R., Edwards, L. & Stelmukh, V. (2006). *Physica B*, **385–386**, 636–638.

Santisteban, J. R., Edwards, L., Steuwer, A. & Withers, P. J. (2001). *J. Appl. Cryst.* **34**, 289–297.

Sato, H. (2018). *J. Imaging*, **4**, 7. **Not cited in text**

Sato, H., Kamiyama, T. & Kiyanagi, Y. (2011). *Mater. Trans.* **52**, 1294–1302.

Strobl, M., Hilger, A., Boin, M., Kardjilov, N., Wimpory, R., Clemens, D., Mühlbauer, M., Schillinger, B., Wilpert, T., Schulz, C., Rolfs, K., Davies, C. M., O'Dowd, N., Tiernan, P. & Manke, I. (2011). *Nucl. Instrum. Methods Phys. Res. A*, **651**, 149–155.

Treimer, W., Strobl, M., Kardjilov, N., Hilger, A. & Manke, I. (2006). *Appl. Phys. Lett.* **89**, 203504.

Vicente Alvarez, M. A., Santisteban, J. R., Domizzi, G. & Almer, J. (2011). *Acta Mater.* **59**, 2210–2220. **Not cited in text**

Vogel, S. (2000). PhD thesis, Christian-Albrechts-Universität zu Kiel, Germany.

Wensrich, C. M., Hendriks, J. N., Gregg, A., Meylan, M. H., Luzin, V. & Tremsin, A. S. (2016). *Nucl. Instrum. Methods Phys. Res. B*, **383**, 52–58.

Woracek, R., Penumadu, D., Kardjilov, N., Hilger, A., Boin, M., Banhart, J. & Manke, I. (2014). *Adv. Mater.* **26**, 4069–4073.

Woracek, R., Santisteban, J., Fedrigo, A. & Strobl, M. (2018). *Nucl. Instrum. Methods Phys. Res. A*, **878**, 141–158.

JOURNAL OF APPLIED CRYSTALLOGRAPHY

ISSN: 1600-5767

ORDER FORM

YOU WILL AUTOMATICALLY BE SENT DETAILS OF HOW TO DOWNLOAD AN ELECTRONIC REPRINT OF YOUR PAPER, FREE OF CHARGE. PRINTED REPRINTS MAY BE PURCHASED USING THIS FORM.

Please scan your order and send to ls@iucr.org

INTERNATIONAL UNION OF CRYSTALLOGRAPHY
5 Abbey Square
Chester CH1 2HU, England.

VAT No. GB 161 9034 76

Article No.: J210386-VG5133

Title of article A novel method to obtain integral parameters of the orientation distribution function of textured polycrystals from wavelength-resolved neutron transmission spectra

Name Miguel Angel Vicente Alvarez

Address Laboratorio Argentino de Haces de Neutrones, Comisión Nacional de Energía Atómica CNEA/CONICET, 9500 Bustillo, SC de Bariloche, Rio Negro, 8400, Argentina

E-mail address (for electronic reprints) m.a.vicente@cab.cnea.gov.ar

OPEN ACCESS

IUCr journals offer authors the chance to make their articles open access on **Crystallography Journals Online**. If you wish to make your article open access please go to https://scripts.iucr.org/openaccess/?code=VG5133

The charge for making an article open access is from **1600 United States dollars** (for full details see https://journals.iucr.org/j/services/openaccess.html). For authors in European Union countries, VAT will be added to the open-access charge.

DIGITAL PRINTED REPRINTS

I wish to order . . . . . paid reprints

These reprints will be sent to the address given above. If the above address or e-mail address is not correct, please indicate an alternative:

PAYMENT (REPRINTS ONLY)

Charge for reprints . . . . . USD

☐ An official purchase order made out to **INTERNATIONAL UNION OF CRYSTALLOGRAPHY** ☐ is enclosed ☐ will follow

Purchase order No.

☐ Please invoice me

☐ I wish to pay by credit card

EU authors only: VAT No:

Date | Signature

OPEN ACCESS

The charge for making an article open access is from **1600 United States dollars** (for full details see https://journals.iucr.org/j/services/openaccess.html). For authors in European Union countries, VAT will be added to the open-access charge.

DIGITAL PRINTED REPRINTS

An electronic reprint is supplied free of charge.

Printed reprints without limit of number may be purchased at the prices given in the table below. The requirements of all joint authors, if any, and of their laboratories should be included in a single order, specifically ordered on the form overleaf. All orders for reprints must be submitted promptly.

Prices for reprints are given below in **United States dollars** and include postage.

	Size of paper (in printed pages)				
Number of reprints required	1–2	3–4	5–8	9–16	Additional 8's
50	184	268	372	560	246
100	278	402	556	842	370
150	368	534	740	1122	490
200	456	664	920	1400	610
Additional 50's	86	128	178	276	116

PAYMENT AND ORDERING

Open-access fees should be paid at https://scripts.iucr.org/openaccess/?code=VG5133

Official purchase orders should be made out to **INTERNATIONAL UNION OF CRYSTALLOGRAPHY**.

Orders should be returned by email to ls@iucr.org

ENQUIRIES

Enquiries concerning reprints should be sent to support@iucr.org.